http://dx.doi.org/10.5012/bkcs.2014.35.11.3181

CoMSIA 3D-QSAR Analysis of 3,4-Dihydroquinazoline Derivatives Against Human Colon Cancer HT-29 Cells

Gi Hyun Kwon, Sehyeon Cho, Jinsung Lee, Joo Mi Sohn, Joon Seok Byun, Kyung-Tae Lee,† and Jae Yeol Lee*

*Research Institute for Basic Sciences and Department of Chemistry, College of Sciences, Kyung Hee University, Seoul 130-701, Korea. *E-mail: ljy@khu.ac.kr*
†Department of Life and Nanopharmaceutical Science, Kyung Hee University, Seoul 130-701, Korea
Received May 12, 2014, Accepted July 2, 2014

A series of 3,4-dihydroquinazoline derivatives with anti-cancer activities against human colon cancer HT-29 cell were subjected to three-dimensional quantitative structure-activity relationship (3D-QSAR) studies using the comparative molecular similarity indices analysis (CoMSIA) approaches. The most potent compound, **BK10001** was used to align the molecules. As a result, the best prediction was obtained with CoMSIA combined electrostatic, hydrophobic, and hydrogen-bond acceptor fields (q^2 = 0.648, r^2 = 0.882). This model was validated by an external test set of six compounds giving satisfactory predictive r^2 values of 0.879. This model would guide the design of potent 3,4-dihydroquinazoline derivatives as anti-cancer agent for the treatment of human colon cancer.

Key Words : CoMSIA, 3D-QSAR, 3,4-Dihydroquinazoline, Human colon cancer

Introduction

Calcium is an essential signal transduction element in the cell cycle progression.[1] Control of intracellular Ca^{2+} is crucial for the orderly progression of the cell cycle and plays a vital role in the regulation of cell proliferation and growth.[2,3] Thus, alterations in calcium signalling can cause defects in cell growth and invasion, and are associated with certain types of cancer.[4,5] Among calcium channels, T-type Ca^{2+} channels (a low voltage-activated Ca^{2+} channel) play a potential role in the regulation of tumor growth and progression.[6] There is a lot of evidence suggesting that the T-type Ca^{2+} channels are abnormally expressed in cancerous cells and that blockade of these channels may reduce cell proliferation in addition to inducing apoptosis.[7-11] Recently, we reported that T-type Ca^{2+} channel blockers, 3,4-dihydroquinazoline derivatives, had both *in vitro* and *in vivo* potent anti-tumor activity against human cancer cells, such as lung cancer A549, pancreatic cancer MiaPaCa2, colon cancer HT-29, and ovarian cancer SK-OV-3 cells.[12-18]

3D-QSAR techniques, such as comparative molecular force field analysis (CoMFA) and comparative molecular similarity indices analysis (CoMSIA), have been developed and widely used in medicinal chemistry.[19] The CoMFA program places the drug molecules with a steric or an electrostatic probe at evenly spaced grid points.[20] The CoMSIA program is known as one of the new 3D QSAR descriptors. In CoMSIA, the steric (abbreviation: S) and electrostatic features (abbreviation: E), hydrogen-bond donor (abbreviation: D), hydrogen-bond acceptor (abbreviation: A) and hydrophobic fields (abbreviation: H) are considered.[21,22] Thus, the CoMSIA program could supply better information than CoMFA program for designing new compounds or potential drug candidates.

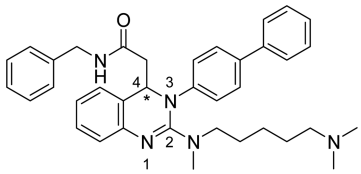

Figure 1. Structure of representative 3,4-dihydroquinazoline (**1**: **BK10001**).

As a continuous strategy to improve the cytotoxic effect of 3,4-dihydroquinazoline derivatives on human colon cancer HT-29 cells (Figure 1),[12] therefore, we have performed the 3D-QSAR studies on these compounds by CoMSIA method, which produces three-dimensional model to indicate the regions that affect biological activity with the change in chemical substitution.

Experimental

Among the library of 3,4-dihydroquinazoline compounds prepared by our group, 37 compounds showing a wide range of cytotoxicities (IC_{50} values of 1.46 to 97.6 μM) against human colon cancer HT-29 cells were selected for the present study. The cytotoxic effects (IC_{50} data) on human colon cancer HT-29 cells were converted to pIC_{50} ($-\log IC_{50}$) values and used for CoMSIA analysis (Table 1). 31 compounds were used as the training set and the remaining 6 compounds were used as the test set to validate the developed CoMSIA model (Table 1).

All molecular modeling calculations were performed using SYBYL-X 1.3 (winnt_os5x).[23] Energy minimizations were performed using Tripos Force Field[24] and Gasteiger-Huckel charge with conjugate gradient method with convergence criterion of 0.05 kcal/mol. As no structural infor-

Table 1. Structures, actual and predicted inhibitory activities of 3,4-dihydroquinazoline derivatives

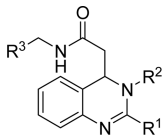

(**1-18**, **20-37**)

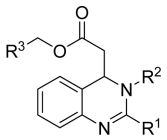

(**19**)

Entry	R^1	R^2	R^3	Actual pIC_{50}[a,b]	Pred. pIC_{50}	Residual
Training set						
1	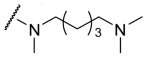	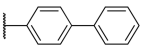		5.84	5.76	-0.08
2	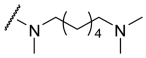	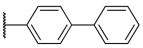		5.83	5.86	0.03
3	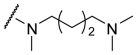	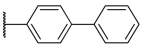		5.59	5.69	0.09
4	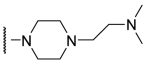	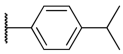		5.52	5.28	-0.24
5	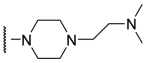	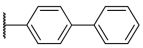	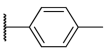	5.47	5.56	0.09
6	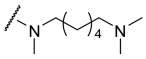	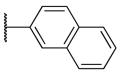		5.47	5.55	0.08
7	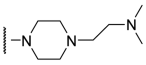	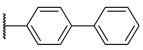	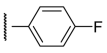	5.43	5.52	0.09
8	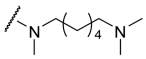	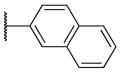	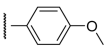	5.43	5.36	-0.07
9	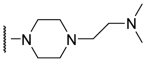	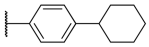		5.40	5.29	-0.11
10	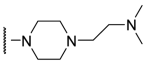	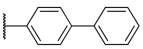	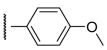	5.38	5.37	-0.01
11	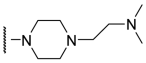	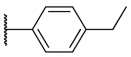	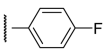	5.38	5.22	-0.16
12	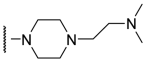	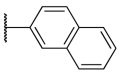		5.36	5.34	-0.02
13	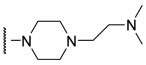	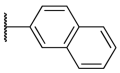	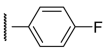	5.30	5.28	-0.02
14	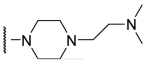	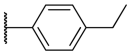		5.30	5.28	-0.02
15	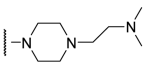	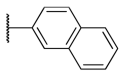	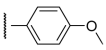	5.24	5.10	-0.14
16	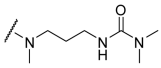	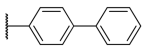		5.22	5.02	-0.20
17	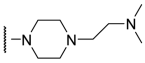	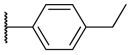	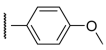	5.24	5.18	-0.06
18	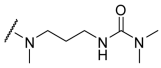	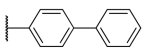	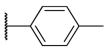	5.18	5.08	-0.10
19	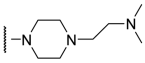	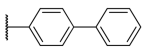		5.16	5.49	0.33

Table 1. Continued

Entry	R^1	R^2	R^3	Actual pIC_{50}[a,b]	Pred. pIC_{50}	Residual
Training set						
20	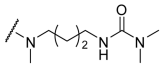	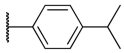	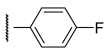	5.01	4.89	-0.12
21	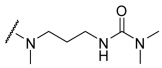	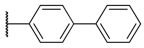	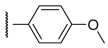	5.00	4.83	-0.17
22	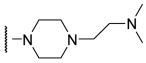	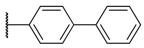		4.97	5.07	0.10
23	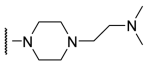	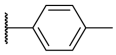		4.95	5.21	0.26
24	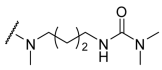	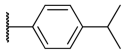		4.90	4.98	0.08
25	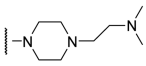	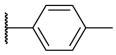	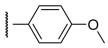	4.90	4.92	0.02
26	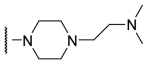	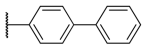	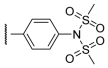	4.74	4.67	-0.07
27	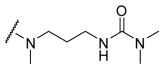	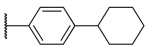		4.69	4.64	-0.05
28	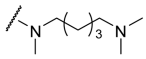	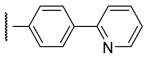		4.43	4.35	-0.08
29	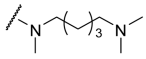	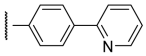		4.34	4.55	0.21
30	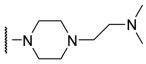	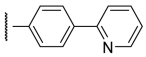		4.34	4.30	-0.04
31	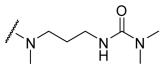	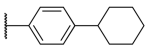	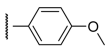	4.01	4.40	0.39
Test set						
32	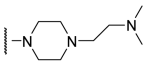	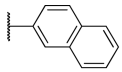	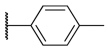	5.62	5.38	-0.24
33	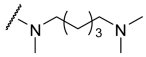	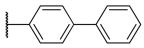	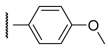	5.42	5.51	0.09
34	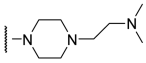	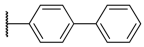		5.35	5.32	-0.03
35	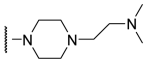	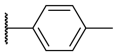		5.14	5.17	0.03
36	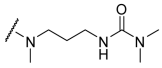	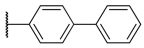	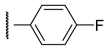	4.99	5.01	0.02
37	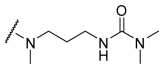	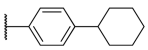	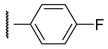	4.69	4.69	0.00

[a]IC_{50} values were measured by MTT assay. [b]$pIC_{50} = -\log IC_{50}$.

mation is available about ligand–receptor complexes for T-type calcium channel, the minimum energy conformation of **1** (**BK10001**: lowest IC_{50} value) *via* simulated annealing protocol (heating molecule at 700 K for 1000 fs and annealing molecule to 200 K for 1000 fs) was used as a template to align the selected compounds assuming that this template is

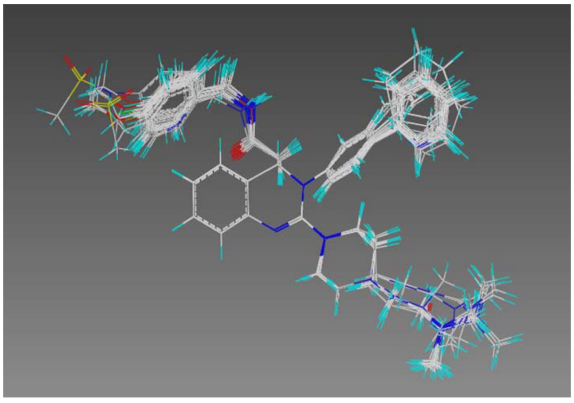

Figure 2. Alignments based on minimum energy conformation of **1** (**BK10001**).

a bioactive conformation.[20] In particular, this conformation was obtained based on arbitrary *S* configuration at 4-position of **1** (**BK10001**) as shown in Figure 1 because all 3,4-dihydroquinazoline derivatives were prepared as racemates and thus this arbitrary *S* configuration was used for the other molecules. We aligned the molecules using this template as shown in Figure 2. CoMSIA descriptors were derived according to Klebe *et al.*[21] Each potential field for CoMSIA was calculated at each lattice intersection of a regularly spaced grid of 2.0 Å and attenuation factor of 0.3. The regression analysis of the CoMSIA field energies was performed using PLS (partial least squares) with LOO (leave-one-out) cross-validation. In CoMSIA analysis, the five different descriptor fields are not totally independent of each other.[25,26] Therefore, some possible combinations of different fields were performed to determine the best CoMSIA model.

Results and Discussion

The summary of the statistical results obtained for CoMSIA studies is shown in Table 2. To validate the predictive power of the model derived using the training set, the biological activities of the test set molecules were predicted. The predictive ability of the model is expressed by the predictive r^2 value. The predictive ability of the CoMSIA model was determined from a set of 6 test compounds not included in the model generation. As a result, both good cross-validated q^2 (0.648) and predicted r^2_{pred} (0.879) values were obtained by using the combination of electrostatic (E), hydrophobic (H) and hydrogen-bond acceptor (A) fields with four components. The corresponding field contributions are 24%, 46%, and 30%, respectively, as shown in Table 2 and 3.

The scrambling stability test represents a second internal method to ensure the validity of 3D-QSAR models.[27] QSAR models which are unstable (that is, which change greatly with small changes in underlying response values) are characterized by slopes ($dq^{2'}/dr^2yy'$) greater than 1.20. Stable models (that is, which change proportionally with small changes in underlying data) have slopes near unity. To investigate the risk of chance correlations, the potencies of the 31 compounds were randomly scrambled and the q^2

Table 4. The summary of scrambling stability test

No. of components	Q^2	cSDEP	$dq^{2'}/dr^2yy'$
2	0.431	0.339	0.895
3	0.497	0.324	1.015
4	0.540	0.316	1.084
5	0.494	0.336	1.309
6	0.466	0.352	1.552

$Q^2 = 1 - (cSDEP)^2$, the predictivity of the model after potential effects of redundancy have been removed, that is, the expected value of q^2 at the specified critical point.; cSDEP, scaled cross-validated standard error (SDEP normalized by the standard deviation of the dependent variables); $dq^{2'}/dr^2yy'$, the slope of q^2 with respect to the correlation of the original dependent variables versus the perturbed dependent variables.

Table 2. Combination of different CoMSIA fields and their results

Parameter	HAD	SED	SEA	SHE	EHA	EHD	SEDA	SEHD	SEHA	SEHDA
q^2	0.655	0.272	0.562	0.538	**0.648**	0.548	0.503	0.508	0.640	0.592
N	5	4	4	4	**4**	3	5	3	4	4
SEP	0.279	0.398	0.308	0.317	**0.276**	0.307	0.335	0.341	0.280	0.298
r^2	0.904	0.843	0.860	0.908	**0.882**	0.889	0.887	0.873	0.885	0.893
SEE	0.147	0.185	0.175	0.141	**0.160**	0.152	0.159	0.163	0.158	0.152
F	47.314	34.900	39.800	64.036	**48.623**	72.282	39.419	62.130	50.026	54.340
r^2_{pred}	0.735	0.823	0.892	0.731	**0.879**	0.740	0.913	0.724	0.867	0.854

q^2, leave-one-out cross-validated correlation coefficient; N, optimum number of components; SEP, standard error of prediction; r^2, non-cross-validated correlation coefficient; SEE, standard error of estimate; *F*, *F*-test value; r^2_{pred}, predictive correlation coefficient; abbreviations: S, steric; E, electrostatic; H, hydrophobic; D, hydrogen-bond donor; A, hydrogen-bond acceptor.

Table 3. The summary of optimal PLS (Partial Least Square) analyses

q^2	N	r^2	SEE	*F*	r^2_{pred}	Fraction		
						electrostatic	hydrophobic	acceptor
0.648	4	0.882	0.160	48.623	0.879	0.24	0.46	0.30

q^2, leave-one-out cross-validated correlation coefficient; N, optimum number of components; r^2, non-cross-validated correlation coefficient; SEE, standard error of estimate; *F*, F-test value; r^2_{pred}, predictive correlation coefficient; Fraction, relative contributions of each CoMSIA descriptor.

values were calculated using LOO cross-validation. Again, the scrambling stability test has to be repeated several times to avoid chance results. According to the results presented in Table 4, five cases (2, 3, 4, 5 and 6-component models) showed the acceptable range values of $dq^{2'}/dr^2yy'$. Among them, 4-component model is most reliable because it showed the highest Q^2 value (0.540), the lowest cSDEP (0.316) and the nearest $dq^{2'}/dr^2yy'$ value to unity. It also coincides with the result of PLS analyses.

Contour maps of CoMISA models can provide useful information to understand the key structural features responsible for the activity. The contour maps of the CoMSIA electrostatic, hydrophobic and hydrogen bond acceptor fields are presented in Figure 3. The favored and disfavored levels are fixed at 80% and 20% in each contour map. For simple comparison, the interactions between the most and least active compounds **1** (**BK10001**) and **31**, and the contour map are shown in Figure 3. The representation illustrated in Figure 3(a) and (b) shows the electrostatic maps contribution of the best model generated by CoMSIA, in which the blue and red contours correspond to regions where an increase in positive or negative charge, respectively, will enhance the activity. Two blue contours are mainly located at the 2-position of R^2 phenyl ring and the 4-position of R^3 phenyl ring. The pyridine rings of R^2 substituents in compounds **28-30** fall in one of two regions, it is probably one of the structural reasons for the decreased activity of these compounds (pIC_{50} 4.34-4.43) compared to compound

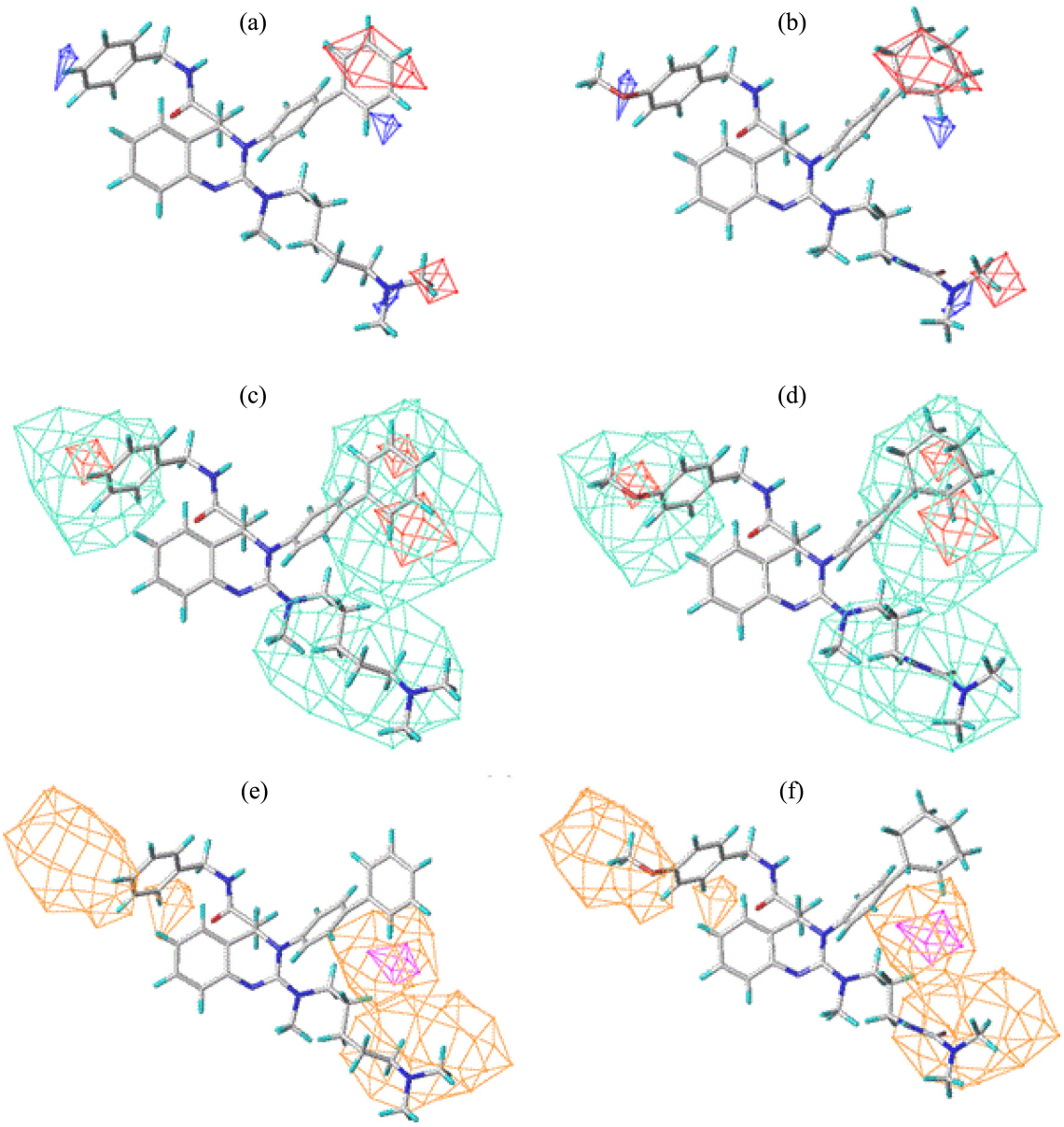

Figure 3. CoMSIA contour plots with **1** (**BK10001**) and **31**. (a) Electrostatic field. Blue and red contours indicate regions where positive and negative charge favors activity, respectively. (b) Hydrophobic field. Red-orange and green-blue contours indicate regions that hydrophobic and hydrophilic group favors activity, respectively. (c) Hydrogen-bond acceptor field. Magenta and orange contours indicate regions where hydrogen-bond acceptor favors and disfavors activity, respectively.

1 (pIC_{50} 5.84). The 4-fluoro- and 4-methoxyphenyl rings of R^3 substituents in compounds **20** and **31** fall in the other of two regions, which accounts for the relative low activities of these compounds (pIC_{50} 5.01 and 4.01). Large red contour is around one phenyl of biphenyl ring in compound **1**, suggesting the importance of phenyl ring (electron-rich group) for its high activity when compared to the low activities of **14** (ethyl), **23** (methyl), **20** (isopropyl), and **31** (cyclohexyl). Small red contour corresponds to 6-nitrogen atom in R^1 substituent of compound **2** (not shown here) and justifies the high activity of compound **2** (pIC_{50} 5.83) comparable to reference compound **1**.

In Figure 3(c) and (d), red-orange and green-blue contours show that hydrophobic and hydrophilic group increases activity, respectively. These contours gave more contribution (46%) to the QSAR equation than the other fields. Three red-orange contours are shown at the end parts of R^2 and R^3 substituents. One red-orange contour at R^3 substituent coincides with the positive region of electrostatic contours at the same positions. Two red-orange contours around the phenyl ring at R^2 position of compound **1** indicate the poor activities of pyridine ring-containing compounds (**28-30**, pIC_{50} 4.34-4.43) and small methyl group-containing compounds (**23** and **25**, pIC_{50} 4.95 and 4.90), respectively. Three large green-blue (hydrophilic favored) contours are shown around R^1-R^3 substituents, respectively. Hydrophilic α,ω-diaminoalkane chain or 4-(2-dimethylaminoethyl)piperazine ring corresponds to the contour of R^1 substituent. 2-Naphthyl (compound **6**, pIC_{50} 5.47) or biphenyl ring instead of alkyl-substituted phenyl ring corresponds to the contour of R^2 substituent. Finally, 4-fluorophenyl (compound **7**, pIC_{50} 5.43) or 4-methoxyphenyl ring (compound **8**, pIC_{50} 5.43) instead of simple phenyl ring corresponds to the contour of R^3 substituent.

Contours favored by hydrogen-bond acceptor are shown in magenta and unfavorable contours were in orange, respectively (Figure 3(e) and (f)). The small favored magenta contour is located at the 4-position (nitrogen atom) of the piperazine ring at R^2 substituent (not shown here), which can be associated with the higher activity of most of the piperazine-containing derivatives (**4-5**, **7**, and **9-15**: $pIC_{50} > 5.24$). Three large unfavored orange contours are shown at all R^1-R^3 substituents. Two large contours correspond to the ureido group (less active compound **27** and **31** pIC_{50} 5.69 and 4.01) at R^1 substituent and the pyridine ring (less active compounds **28-30** $pIC_{50} < 4.5$) at R^2 substituent, respectively. Finally, two orange contours are seen at the region of R^3 substituent, which corresponds to 2-pyridine ring (compound **28** pIC_{50} 4.43), bis(sulfonamide) group (compound **26** pIC_{50} 4.74), and 4-methoxyphenyl group (compound **31** pIC_{50} 4.01).

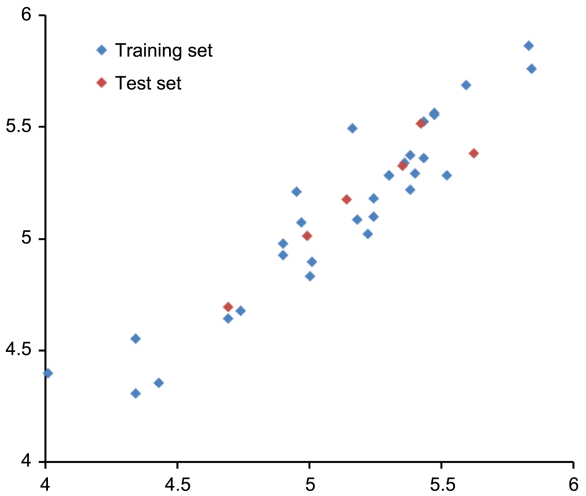

Figure 4. Actual versus predicted pIC_{50} of training and test set molecules.

Figure 4 shows plots of actual vs. predicted activities of training and test sets of CoMSIA. Blue diamond shows the predictions of the training set and red shows that of test set. The actual and predicted value of the training and test set molecules showed a linear relationship. The predictive r^2 value of the test set is 0.884.

Conclusion

In conclusion, CoMSIA studies on thirty-seven 3,4-dihydroquinazoline derivatives were carried out to develop a 3D-QSAR model that provided good predictivity for the training set ($q^2 = 0.648$, $r^2 = 0.882$) and the test set ($r^2_{pred} = 0.879$). The information obtained CoMSIA 3D-maps can be used for the design of new chemical entities with high anticancer activity against human colon cancer HT-29 cells.

Acknowledgments. This research was supported by Basic Science Research Program through the National Research Foundation of Korea (NRF) funded by the Ministry of Education (NRF-2013R1A1A2058915).

References and Notes

1. Machaca, K. *Cell Calcium* **2011**, *49*, 323.
2. Berridge, M. J.; Lipp, P.; Bootman, M. D. *Nat. Rev. Mol. Cell Biol.* **2000**, *1*, 11.
3. Berridge, M. J.; Bootman, M. D.; Roderick, H. L. *Nat. Rev. Mol. Cell Biol.* **2003**, *4*, 517.
4. Santoni, G.; Santoni, M.; Nabissi, M. *Br. J. Pharmacol.* **2012**, *166*, 1244.
5. Zhang, Y.; Zhang, J.; Jiang, D.; Zhang, D.; Qian, Z.; Liu, C.; Tao, J. *Br. J. Pharmacol.* **2012**, *166*, 1247.
6. Panner, A.; Wurster, R. D. *Cell Calcium* **2006**, *40*, 253.
7. Perez-Reyes, E. *Physiol. Rev.* **2003**, *83*, 117.
8. Li, M.; Xiong, Z.-G. *Int. J. Physiol. Pathophysiol. Pharmacol.* **2011**, *3*, 156.
9. Latour, I.; Louw, D. F.; Beedle, A. M.; Hamid, J.; Sutherland, G. R.; Zamponi, G. W. *Glia* **2004**, *48*, 112.
10. Taylor, J. T.; Zeng, X.-B.; Pottle, J. E.; Lee, K.; Wang, A. R.; Yi, S. G.; Scruggs, J. A.; Sikka, S. S.; Li, M. *World J. Gastroenterol.* **2008**, *14*, 4984.
11. Li, W.; Zhang, S.-L.; Wang, N.; Zhang, B.-B.; Li, M. *Cancer Invest.* **2011**, *29*, 339.
12. Heo, J. H.; Seo, H. N.; Choe, Y. J.; Kim, S.; Oh, C. R.; Kim, Y. D.; Rhim, H.; Choo, D. J.; Kim, J.; Lee, J. Y. *Bioorg. Med. Chem. Lett.* **2008**, *18*, 3899.
13. Jung, S. Y.; Lee, S. H.; Kang, H. B.; Park, H. A.; Chang, S. K.; Kim, J.; Choo, D. J.; Oh, C. R.; Kim, Y. D.; Seo, J. H.; Lee, K.-T.; Lee, J. Y. *Bioorg. Med. Chem. Lett.* **2010**, *20*, 6633.

14. Kang, H. B.; Rim, H. K.; Park, J. Y.; Choi, H. W.; Choi, D. L.; Seo, J. H.; Chung, K. S.; Huh, G.; Kim, J.; Choo, D. J.; Lee, K.-T.; Lee, J. Y. *Bioorg. Med. Chem. Lett*. **2012**, *22*, 1198.
15. Rim, H. K.; Lee, H. W.; Choi, I. S.; Park, J. Y.; Choi, H. W.; Choi, J. H.; Cho, Y. W.; Lee, J. Y.; Lee, K.-T. *Bioorg. Med. Chem. Lett*. **2012**, *22*, 7123.
16. Park, J. Y.; Choi, H. W.; Choi, D. L., Jang, S. J.; Kim, J. H.; Lee, J. H.; Choo, D. J.; Kim, J.; Lee, K.-T.; Lee, J. Y. *Bull. Korean Chem. Soc*. **2013**, *34*, 482.
17. Jang, S. J.; Choi, H. W.; Choi, D. L.; Cho, S.; Rim, H. K.; Choi, H. E.; Kim, K. S.; Huang, M.; Rhim, H.; Lee, K.-T.; Lee, J. Y. *Bioorg. Med. Chem. Lett*. **2013**, *23*, 6656.
18. Choi, D. L.; Jang, S. J.; Cho, S.; Choi, H. E.; Rim, H. K.; Lee, K.-T.; Lee, J. Y. *Bioorg. Med. Chem. Lett*. **2014**, *24*, 1565.
19. Verma, J.; Khedkar, V. M.; Coutinho, E. C. *Curr. Top. Med. Chem*. **2010**, *10*, 95.
20. Cramer, R. D.; Patterson, D. E.; Bunce, J. D. *J. Am. Chem. Soc*. **1988**, *110*, 5959.
21. Klebe, G.; Abraham, U.; Meitzner, T. *J. Med. Chem*., **1994**, *37*, 4310.
22. Klebe, G.; Abraham, U. *J. Comput-Aided Mol. Des*. **1999**, *13*, 1.
23. SYBYL-X 1.3. Tripos Associates Inc.: 1699 S. Hanley Rd., St. Louis, MO 631444, USA.
24. Clark, M.; Cramer III, R. D.; Van Opdenbosch, N. *J. Comput. Chem*. **1989**, *10*, 982.
25. Bringmann, G.; Rummey, C. *J. Med. Chem*. **1999**, *42*, 458.
26. Bringmann, G.; Rummey, C. *J. Chem. Inf. Comput. Sci*. **2003**, *43*, 304.
27. Pick, A.; Müller, H.; Wiese, M. *Bioorg. Med. Chem*. **2008**, *16*, 8224.